Thermal Load on Wirescanners in the FLASH Linac

— DESY Technical Note 2006-02 —

Lars Fröhlich, MPY

2006/07/31
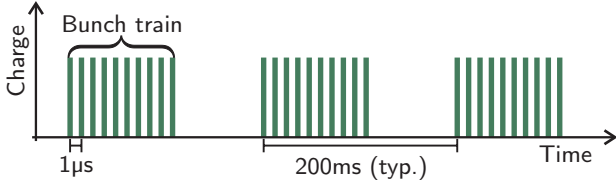
Figure 1: Time structure of the FLASH beam for exemplary parameters of $N = 10$, $\nu_{\text{bunch}} = 1\,\text{MHz}$, $\nu_{\text{macropulse}} = 5\,\text{Hz}$

1 Introduction

The FLASH linac transports electron bunches with a charge of typically 1 nC. As shown in Fig. 1, a number N of these bunches is released from the photocathode RF gun with a frequency ν_{bunch}, forming a macropulse or bunch train. These macropulses are repeated at a repetition rate $\nu_{\text{macropulse}}$. Up to now, typical operation parameters have been the following:

N	1 to 30
ν_{bunch}	1 MHz, 250 kHz, 100 kHz
$\nu_{\text{macropulse}}$	5 Hz, 2 Hz, 1 Hz

At FLASH, wirescanners are used in several locations for beam size and position diagnostics. With the time structures mentioned above, thermal load on the wires has not been an issue. However, the linac specification foresees macropulses of up to 800 bunches with a repetition rate of 10 Hz, or in a later step even 7200 bunches at $\nu_{\text{bunch}} = 9\,\text{MHz}$. First tests of operation with longer pulses necessitate a closer examination of the thermal stress. The approach described in this note is a numerical simulation including heat conduction and heat radiation effects.

1.1 Wire types

Two types of wirescanners are used at FLASH. Eight devices in the sections DBC2, DBC3, ECOL, MATCH, BYPASS have been built by MDI using 15 μm thick tungsten wires. The undulator is equipped with seven wirescanners developed by DESY Zeuthen [Cas05]. These installations carry three different wires each, 10 μm graphite as well as 10 and 50 μm tungsten.

2 Simulation method

The wire is modeled as a 5 cm long cylinder of the pure wire material in perfect vacuum. In contrast to a real wire, it has no thermal contact to an outer heat reservoir, making the simulation describe a worst case scenario with respect to heat conduction. The simulation proceeds in time steps of variable length Δt_i, and the wire is spatially divided into J segments of variable length Δl_j.

At the simulation start, all wire segments have a uniform temperature of 270 K. In each time step i, the individual heat balance $Q_{i,j}$ is computed for each segment j. Beside the thermal energy deposited by the passing bunches, heat conduction and "graybody" radiation are taken into account.

The temperature change of the segments is then calculated from the specific heat capacity $c_p(T)$ and the mass of the wire segments:

$$T_{i,j} = T_{i-1,j} + \frac{Q_j}{c_p(T_{i-1,j}) \cdot \pi \frac{d^2}{4} \Delta l_j \cdot \rho}$$

2.1 Heating by scattering of the beam

During a scan, the wire successively gets in contact with several bunches. Most of the time, the overlap is limited to an outer part of the electron cloud, and the contribution to the heat load on the material is marginal. To simplify the treatment, we will therefore consider only central impacts of the particle bunches onto the wire. In this way, we obtain the maximum possible transfer of heat between the two systems for each impact.

The heat Q^{beam} deposited in the wire can be approximated roughly by calculating the ionization energy loss with the Bethe-Bloch formula [Wit00a]. With the number of particles per bunch N_{b},

$$Q \approx 0.3 N_{\text{b}} \frac{d^2}{2\sigma} \rho \frac{\text{d}E}{\text{d}x}, \tag{1}$$

where d is the thickness of the wire and ρ the density of the material. The factor of 0.3 is based on the assumption that about 70 % of the heat is carried away by secondary particles [Bos86]. The coefficient $\text{d}E/\text{d}x$ describes the mean rate of energy loss due to ionization and is calculated with the Bethe-Bloch formula as given

Material	ρ (g/cm^3)	dE/dx (MeV cm^2 g^{-1})
Tungsten	19.26	1.75
Graphite	2.2	2.13

Table 1: Density and specific ionization energy loss used in the calculations; $\mathrm{d}E/\mathrm{d}x$ has been calculated for electrons of 450 MeV.

Wire type	Approximation Q (µJ)	Monte Carlo Q (µJ)
10 µm graphite	0.140	0.169 ± 0.002
10 µm tungsten	1.01	2.19 ± 0.04
15 µm tungsten	2.27	4.90 ± 0.05
50 µm tungsten	25.3	32.0 ± 0.1

Table 2: Heat deposited in various wire types by a passing bunch of 1 nC. The approximated value follows (1), the "Monte Carlo" result is obtained by the simulation of an electromagnetic shower with Fluka.

in [PDG04], with an approximation for the atomic excitation potential from [Leo94]. The coefficients for a beam energy of 450 MeV are summarized in Tab. 1.

For comparison, a Monte-Carlo simulation of the electromagnetic shower has been carried out with the transport code Fluka [Fer05]. The deposited energies obtained with both methods for a bunch charge of 1 nC and a transverse rms beam width of $\sigma = 50\,\mu\mathrm{m}$ are of the order of microjoules (Tab. 2). Since the approximated values are systematically too low, it is possible that the assumed rate of heat transfer by secondary particles is too big. However, the trend of the results for the various wire types is in agreement between both methods. Only the Monte-Carlo results are used for further calculations.

When a bunch passes the wire in the simulation, the fixed amount of heat Q^{beam} calculated before is distributed to the wire segments corresponding to the transverse beam profile, which is assumed to be a Gaussian of width σ.

2.2 "Graybody" radiation

For the calculation of radiative energy losses, the wire is treated as a "graybody". This means that the emitted spectrum corresponds to that of a blackbody of the same temperature, but with only a fraction of the emitted power. The emissivity ϵ is thus independent of wavelength, and smaller than 1.

In general, ϵ is a function of temperature. As a metal, tungsten has a very low emissivity of $\epsilon_{\mathrm{W}} \approx 0.03$ at room temperature. However, at higher temperatures this value increases to more than 0.35 (see appendix for details), so it is necessary to include the T-dependence in the simulation. For carbon, the situation is simplified by the assumption of a safe lower bound.

The energy radiated during a time step of length Δt_i

is calculated using the Stefan-Boltzmann law:

$$Q_{i,j}^{\mathrm{radiation}} = \epsilon(T_{i-1,j})\sigma A_j T_{i-1,j}^4 \cdot \Delta t_i$$

σ denotes the Stefan-Boltzmann constant, $A_j = \pi d \cdot \Delta l_j$ the surface area of the wire segment.

2.3 Heat conduction

The simulation of thermal conduction is based on Fourier's law, which states that the rate of heat transfer through a contact surface $A_\varnothing$ is proportional to the temperature gradient:

$$\frac{\mathrm{d}Q}{\mathrm{d}t} = -\lambda A_\varnothing \frac{\mathrm{d}T}{\mathrm{d}x}$$

The thermal conductivity λ of the material is a function of the temperature T (see appendix). With the cross-sectional area of the wire $A_\varnothing = \pi d^2/4$, we obtain the following heat flow from wire segment j to wire segment $j+1$:

$$Q_i^{j \to j+1} = \lambda(T_{\mathrm{boundary}})A_\varnothing \frac{T_{i-1,j} - T_{i-1,j+1}}{(\Delta l_j + \Delta l_{j+1})/2}\Delta t_i$$

The temperature of the boundary between the segments is obtained by linear interpolation:

$$T_{\mathrm{boundary}} = \frac{l_{j+1}T_{i,j} + l_j T_{i,j+1}}{l_j + l_{j+1}}$$

3 Results

All simulations have been conducted with a bunch charge of 1 nC and a beam width of 50 µm (rms), which is a reasonable limit for the beam focussing possible at FLASH. Bigger beam sizes are obviously less critical in terms of thermal load on the wires.

Figure 2 presents the build-up of wire temperature during the passing of a single macropulse of 60 bunches at a frequency of 1 MHz. The plot shows the maximum temperature across the wire, in this case the temperature of the central segment. Obviously, the carbon wire has the highest resilience of the four types. It is also discernible that the thin tungsten filaments heat up more rapidly than the thicker one.

3.1 Comparison of cooling mechanisms

As explained before, the two cooling mechanisms simulated by the algorithm are graybody radiation and thermal conduction. The former leads to a direct decrease in temperature of each wire segment, while the latter works by distributing heat energy from local hot spots to neighboring segments. To examine the influence of both mechanisms, a simulation of the 10 µm graphite wire hit by 800 bunches at 1 MHz has been set up. The run has then been executed four times, each one with a different combination of active cooling processes. The results are shown in Fig. 3.
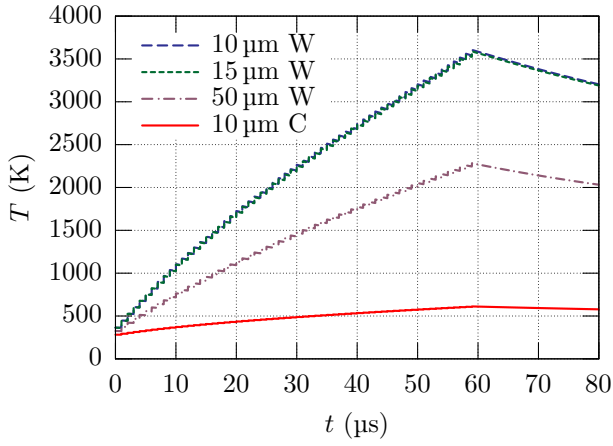
Figure 2: Heating of the four wire types by a macropulse with 60 bunches at a bunch frequency of 1 MHz
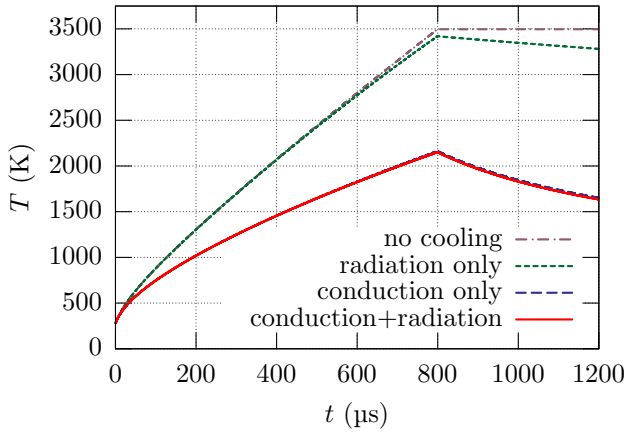
Figure 3: 10 µm graphite wire bombarded with 800 bunches at 1 MHz; simulated with various combinations of cooling mechanisms
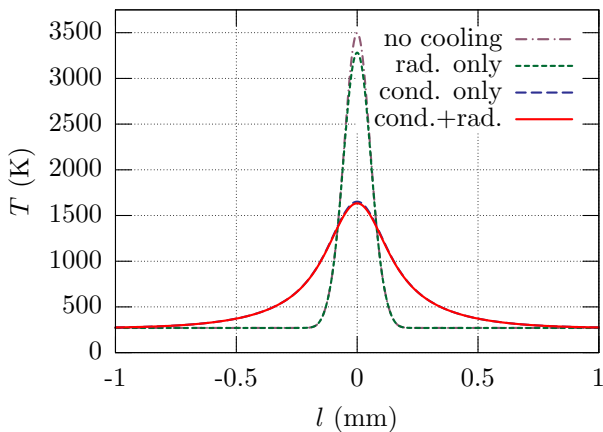
Figure 4: Temperature distributions for a 10 µm graphite wire, 400 µs after the impact of the last of 800 bunches at 1 MHz; simulated with various combinations of cooling mechanisms

	100 kHz	1 MHz	9 MHz	
5 Hz	∞	1974	976	**10 µm**
10 Hz	∞	1833	944	**carbon**
5 Hz	149	54	44	**10 µm**
10 Hz	136	51	43	**tungsten**
5 Hz	141	53	44	**15 µm**
10 Hz	128	50	42	**tungsten**
5 Hz	294	97	75	**50 µm**
10 Hz	254	89	69	**tungsten**

Table 3: Maximum tolerable number of bunches per macropulse for the four wire types

While it is sometimes assumed [Lef78, Wit00a] that thermal conduction is generally negligible in the treatment of heat load on wirescanners, the obtained temperature curves make it clear that this is not the case for the time structure of a superconducting linac. In fact, *thermal conduction is the dominant cooling mechanism.* This holds true for the tungsten wires as well, regardless of thickness or choice of material parameter sets.

Figure 4 shows the corresponding temperature distributions 400 µs after the impact of the last bunch of the macropulse. Even after this comparably short time, the distribution of heat energy has reduced the peak temperature to about half of the value for the runs without thermal conduction.

3.2 Thermal load limits

If too much thermal power is conveyed to a wire, the material will either melt or sublimate. The temperatures assumed critical in the simulation are 3680 K for tungsten, and 3800 K for graphite. The wire might break even at lower temperatures due to dynamic stress, but it is expected that this can be avoided by keeping the duty cycle of the machine sufficiently below the theoretical maximum. Since variations in repetition rate and in bunch frequency both change the heat load on the wire, all the relevant combinations of these parameters have to be covered in an investigation that should yield practical limits for the use of wire scanners.

Table 3 lists the maximum allowed number of bunches per macropulse that keeps the wire slightly below the threshold of breaking for a time of 10 seconds, which is a typical duration for a "slow" wirescan. After this time, most of the simulations have reached a dynamic equilibrium in which the peak temperatures do not rise anymore (Fig. 5).

The repetition rate defines the slow heating of the wire over many macropulses. While the temperature varies over approximately 3000 K between two macropulses, the slow temperature rise is far below 1000 K. Therefore the influence of the repetition rate on the maximum tolerable number of bunches is small.

For these considerations, the bunch frequency is of more importance. For the tungsten wires, a change from 1 MHz to 9 MHz reduces the allowed number of bunches by about 20%. Operation with 100 kHz allows the heat
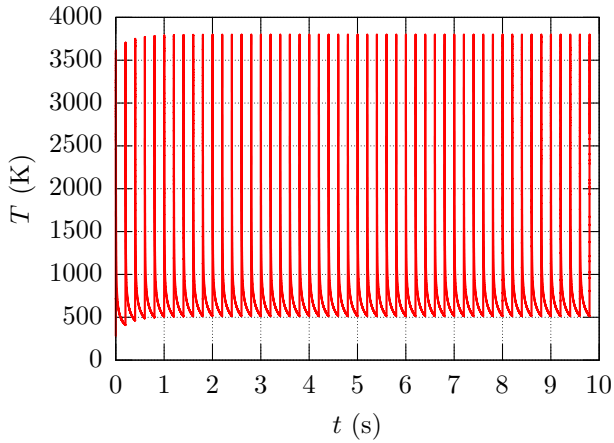
Figure 5: Maximum tolerable heat load in the stress simulation for the $10\,\mu\mathrm{m}$ graphite wire (at $1\,\mathrm{MHz}/5\,\mathrm{Hz}$)

to be spread significantly better between the arrival of two bunches, raising the tolerated number by a factor of three.

Considering the fixed RF pulse length of $800\,\mu\mathrm{s}$ in the FLASH linac, only the operation with $9\,\mathrm{MHz}$ imposes limits on the number of bunches for the graphite wires. Even a permanent bombardment at $100\,\mathrm{kHz}$ only takes the wire into a dynamic equilibrium with a peak temperature of $2170\,\mathrm{K}$. This means that the wire cannot be destroyed by macropulses with this bunch frequency.

4 Conclusion and outlook

Up to now, the use of wirescanners in the FLASH linac has been limited to a maximum of 30 bunches per train. Calculations show that considerably longer macropulses can be tolerated, especially in the case of operation with lower bunch frequencies. The carbon wires employed in the undulator section promise to be an excellent tool for the study of long bunch trains.

In a more sophisticated analysis of the problem, the possibility of wire breakage due to dynamic stress should be included. While the material properties of tungsten are well-known, those of carbon can vary over a wide range. Therefore, a more detailed study of the graphite filaments could increase the accuracy of the simulation.

A more technical point concerns the computing time needed to obtain results with reasonable precision. With the current simple Euler integration algorithm, a typical run over 10 seconds of simulation time takes about 10–30 minutes. The use of a better algorithm like the Runge-Kutta integrator promises to reduce the computing time significantly.

5 Acknowledgements

A Convergence analysis

If the wire segment lengths are chosen too big, the thermal profile induced by the passing beam cannot be resolved with the necessary accuracy, and the peak temperature is underestimated. Because a finer segmentation of the wire results in an increase of computation time, a suitable compromise has to be found.

To check the convergence behavior of the algorithm, several simulation runs have been conducted with the 10 μm carbon wire, bombarded with 100 bunches at a frequency of 1 MHz (rms width 50 μm). Figure 6 shows the maximum temperature of all wire segments across all time steps for various time step widths, coarse and fine segmentations.
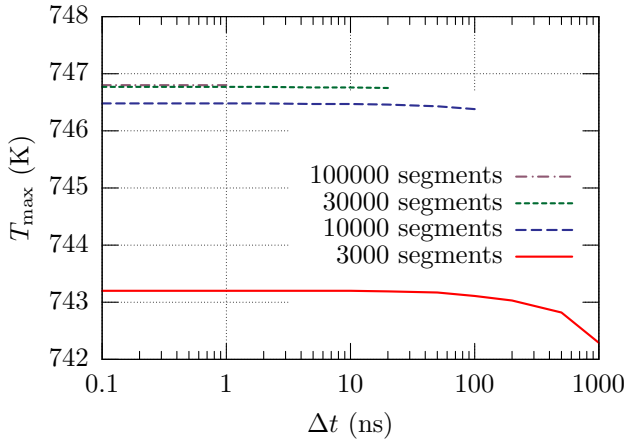
Figure 6: Maximum wire temperature in a simulation run with constant segment lengths for various time step widths

As a main observation, the simulation result is more dependent on the number of segments than on the chosen time step width. However, the choice of Δt is restrained by the onset of a numerical instability; the finer the wire segmentation, the smaller the time step has to be in order to avoid chaotic behavior. This instability also explains the missing points in Fig. 6.

The choice for the number of segments J should be based on the criterion of good sampling of the impact heat profile. In this case, the profile is a Gaussian with 50 μm rms width. Hence, it is clearly undersampled with $J = 3000$, which corresponds to a segment length of $\Delta l = 16.7$ μm. If the segmentation is made finer than $J = 10000$ ($\Delta l = 5$ μm), the simulation result changes by less than 1‰.

A.1 Trapezoidal segmentation

As discussed before, it is important to resolve the fine structures of the thermal profile given by the impact of the bunches in the center of the wire. The outer ends only receive heat from thermal conduction, and therefore the needed spatial resolution is considerably lower. The algorithm can take advantage of this by using non-uniform segment lengths.
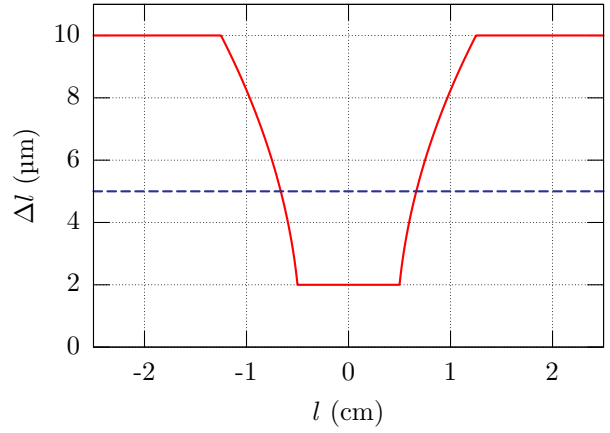
Figure 7: Segment lengths versus wire position for a trapezoidal segmentation compared with uniform segmentation of same J
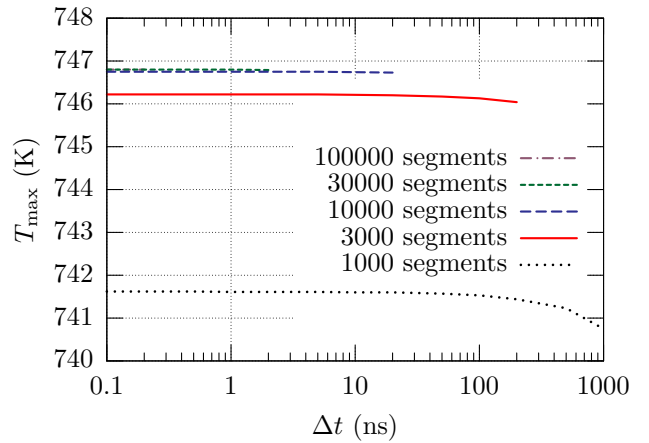
Figure 8: Maximum wire temperature in a the simulation with trapezoidally distributed segment lengths for various time step widths

A trapezoidal segmentation as shown in Fig. 7 increases the local resolution in the center of the wire, and alleviates the demand for high numbers of segments J. Figure 8 shows the results of a convergence analysis for this kind of scale. Compared with the uniform scale discussed above, sufficient accuracy is now already achieved with $J = 3000$, decreasing the overall computation time.

B Material properties

B.1 Specific heat capacity

The specific heat capacity of graphite is considerably higher than that of tungsten, and it increases rapidly from about $600\,\frac{\text{J}}{\text{kg}\cdot\text{K}}$ at room temperature to about $1800\,\frac{\text{J}}{\text{kg}\cdot\text{K}}$ at $1000\,\text{K}$. The data for tungsten is taken from [Kar06], for graphite from [Din91].
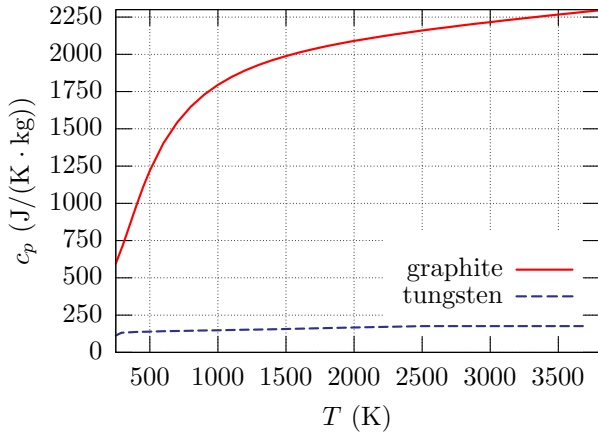
B.2 Thermal conductivity

With T in K, the thermal conductivity of pure tungsten (in $\text{W}/(\text{m}\cdot\text{K})$) is modeled as [Dav97]:

$$k(T) = 174.9274 - 0.1067\,T + 5.0067 \cdot 10^{-5}\,T^2 - 7.8349 \cdot 10^{-9}\,T^3.$$

For the carbon wire, the recommended data set from [Tou78] for ATJ graphite is used. For pure pyrolytic graphite, and for the special case of heat transfer perpendicular to the carbon layers in the crystal, the thermal conductivity is substantially lower; however, this kind of configuration is not to be expected in a carbon wire.
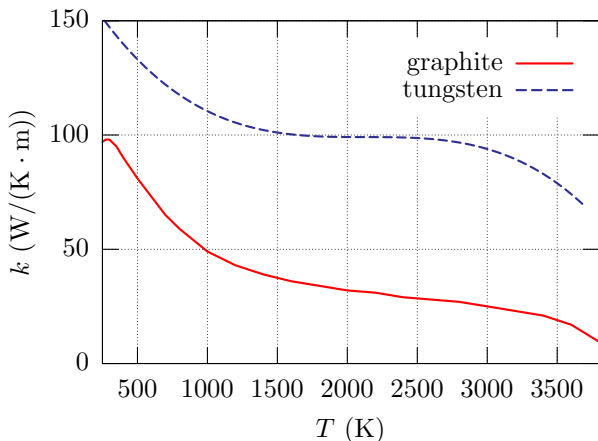
B.3 Emissivity

The emissivity of tungsten is described by the empirical formula

$$\epsilon_{\text{W}}(T) = -0.0434 + 1.8524 \cdot 10^{-4}\,T - 1.954 \cdot 10^{-8}\,T^2$$

if T is given in K [Dav97]. ϵ_{W} is dimensionless.

The total emissivity of graphite depends strongly on the surface properties, and on the thermal and mechanical history of the specific sample. To establish a worst-case scenario, a safe value of $\epsilon_{\text{C}} = 0.6$ is used for all temperatures above $250\,\text{K}$ (compare [Tou70]). ϵ_{C} is set to zero for $T < 250\,\text{K}$ to avoid cooling below this temperature.
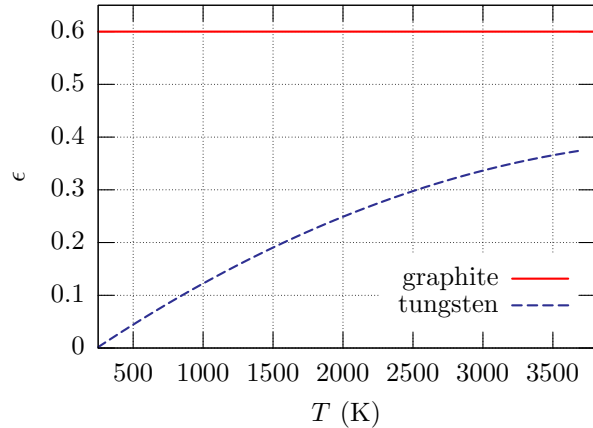
References

[Bos86]   J. Bosser et al. *CERN SPS/86-26 (MS)*. Technical report, 1986.

[Cas05]   P. Castro, H.-J. Grabosch, U. Hahn, et al. *Wire scanners in the undulator section of the VUV-FEL at DESY*. In *Proceedings of DI-PAC 2005*, pp. 205–207. Lyon, France, 2005.

[Dav97]   J. W. Davis, V. Barabash, and S. Fabritsiev. *ITER material properties handbook*, December 1997. URL http://aries.ucsd.edu/LIB/PROPS/ITER/.

[Din91]   A. T. Dinsdale. *SGTE data for pure elements*, 1991. CALPHAD 15.

[Fas03]   A. Fassò, A. Ferrari, S. Roesler, et al. *The physics models of FLUKA: status and recent developments*. In *Proceedings of the Computing in High Energy and Nuclear Physics 2003 Conference (CHEP2003)*. La Jolla, CA, USA, March 2003. Paper MOMT005.

[Fer05]   A. Ferrari, P. R. Sala, A. Fassò, et al. *Fluka: a multi-particle transport code*. CERN, August 2005.

[Kar06]   P. J. Karditsas and M.-J. Baptiste. *Thermal and structural properties of fusion related materials*. URL http://www-ferp.ucsd.edu/LIB/PROPS/PANOS/matintro.html.

[Lef78]   P. Lefèvre. *Mesure très peu destructive des distributions transversales dans le PS de 800 MeV à 26 GeV/c*. CERN internal note CERN/PS/DL/Note 78-8, 1978.

[Leo94]   W. R. Leo. *Techniques for nuclear and parti-
          cle physics experiments: A how-to approach.*
          Springer, Berlin, 2nd edition, 1994.

[PDG04] Particle data group. *Particle physics booklet*,
          July 2004. Extracted from S. Eidelman, et al.,
          Phys. Lett. B 592(1), 2004.

[Tou70]   Y. S. Touloukian (editor). *Thermal radiative
          properties*, *Thermophysical properties of mat-
          ter*, volume 7. IFI/Plenum, New York, 1970.

[Tou78]   Y. S. Touloukian, R. W. Powell, C. Y. Ho,
          et al. (editors). *Thermal conductivity: Non-
          metallic solids*, *Thermophysical properties of
          matter*, volume 2. IFI/Plenum, New York,
          3rd edition, 1978.

[Wit00a] K. Wittenburg. *Conventional wire scanners
          for TESLA*. Tesla report 2000-18, DESY,
          2000.